

# Limits on Activation-Induced Temperature and Metabolic Changes in the Human Primary Visual Cortex

Rachel Katz-Brull, David C. Alsop, Robert P. Marquis, and Robert E. Lenkinski\*

**Changes in cerebral blood flow (CBF) and metabolism are now widely used to map and quantify neural activity, although the underlying mechanism for these changes is still incompletely understood. Magnetic resonance spectroscopy (MRS) at 3T, synchronized with a 32-s block design visual stimulation paradigm, was employed to investigate activation-induced changes in temperature and metabolism in the human primary visual cortex. A marginally significant increase in the local temperature of the visual cortex was found ( $0.1^{\circ}\text{C}$ ,  $P = 0.09$ ), excluding the possibility of a temperature decrease (95% confidence interval (CI) =  $0.0\text{--}0.2^{\circ}\text{C}$ ), which was previously suggested. A comparison with models of thermal equilibrium in the presence of blood flow suggests that an increase in heat production during activation, greater than or at least equal to that produced by the complete oxidative metabolism of the elevated glucose (Glc) utilization accompanying activation, would be required to offset the cooling effects of the increased blood flow. The total pools of glutamate (Glu), glutamine (Gln), myo-Inositol (ml), N-acetylaspartate (NAA), choline (Cho), and lactate (Lac) were not significantly affected by activation. Limits on Lac concentration changes were too weak to constrain theories of the metabolic use of elevated Glc consumption during stimulation, and emphasize the challenges of measuring even large Lac changes accompanying stimulation. Magn Reson Med 56: 348–355, 2006. © 2006 Wiley-Liss, Inc.**

**Key words:** temperature; cerebral blood flow; magnetic resonance spectroscopy; N-acetylaspartate; brain activation

In activated regions of the brain, blood flow and glucose (Glc) consumption increase substantially more than oxygen consumption (1). These changes, along with changes in cerebral blood volume (CBV), lead to the blood oxygenation level-dependent contrast (BOLD) in functional magnetic resonance imaging (fMRI) (1). Both cerebral blood flow (CBF) and metabolism are involved in brain thermoregulation, and pharmacological changes of these processes lead to changes in brain temperature (2). Broad investigations have been concerned with the possible mechanisms that underlie the BOLD effect and its relation to neuronal activation (3). Magnetic resonance spectroscopy (MRS) provides a noninvasive tool to investigate these processes in the conscious human brain, because MRS properties, such as signal area, frequency shift, and line width, can serve as probes of metabolite concentration, temperature, and oxygenation level.

Previous MRS studies used prolonged stimulation duration (4–48 min) (4–9). However, long slow changes are prone to systematic errors. The contribution of drifts to systematic errors can be diminished with the use of a block design paradigm. We chose multiple 32-s blocks as an optimal timing to follow the BOLD response, oxidative Glc metabolism, and anaerobic glycolysis (3,10). The same block design behavioral paradigm was used for both fMRI and MRS studies (at 3T) in order to explore the physiologic and metabolic correlates of brain activation.

## MATERIALS AND METHODS

### Subjects

Nine subjects (five men and four women, 28–57 years of age) underwent MRI, fMRI, and  $^1\text{H}$ -MRS of the brain. Informed consent was obtained in accordance with the guidelines of the Institutional Review Board of the Beth Israel Deaconess Medical Center.

### MRI and Visual Stimulation

The studies were performed on a 3T scanner (Signa VH/i, GE Healthcare, Waukesha, WI) equipped with a transmit body coil and a receive-only 7.8-cm surface coil. The subjects entered the scanner in a supine position, and the calcarine fissure was positioned at the center of the surface coil. Axial  $T_2$ -weighted low flip angle rapid acquisition with relaxation enhancement (RARE) images and EPI  $T_2^*$ -weighted images of the brain were recorded with the same graphic prescription. The EPI data were acquired with a gradient-echo pulse sequence (TR = 2 s, TE = 20 ms, 16 slices, slice thickness = 5 mm). The resulting images were analyzed using Real Time Image Processing (RTIP) software (GE Healthcare). The visual stimulation was delivered through LCD goggles (Resonance Technology, Northridge, CA, USA) equipped with corrective lenses. The visual stimulation paradigm involved 12 repetitions of 40 s of darkness, 32 s of black and white checkerboards alternating at 8 Hz, and 32 s of darkness, with 46 s for rest between the repetitions (with two repetitions for each of the fMRI scans at the start and the end of the study, and 10 repetitions for the MRS investigation). During the rest period the subjects could view a nonchanging light blue screen or rest their eyes by closing them.

### MRS

The MRS voxel ( $2 \times 2 \times 1$ ,  $4 \text{ cm}^3$ ) was positioned on the  $T_2$ -weighted images at the site of activation observed in the RTIP images. The spectra were acquired using a point-resolved spectroscopy (PRESS) sequence with a TR of 2 s, short TE of 35 ms, spectral width of 5000 Hz, 2048 time points, partial water suppression, and a localization gra-

Department of Radiology, Beth Israel Deaconess Medical Center and Harvard Medical School, Boston, Massachusetts, USA.

\*Correspondence to: Robert E. Lenkinski, Ph.D., Professor, Harvard Medical School, Associate Chief for Academic Affairs, Director of Experimental Radiology, Director 3T MRI/MRS Program, Department of Radiology, Beth Israel Deaconess Medical Center, 330 Brookline Ave., Boston, MA 02215. E-mail: rlenkins@bidmc.harvard.edu

Received 21 December 2005; revised 13 April 2006; accepted 27 April 2006.  
DOI 10.1002/mrm.20972  
Published online 21 June 2006 in Wiley InterScience (www.interscience.wiley.com).

dient order of sagittal-axial-coronal. The MRS acquisition was synchronized to the stimulation paradigm and the spectral frames were stored individually. The free induction decays (FIDs) were zero-filled to 8192 points before they were processed.

#### Frequency Variations, Temperature, and $T_2^*$ Determination

The change in temperature was calculated based on the shift in the resonance frequency of the water signal. Because the resonance frequency of the NAA methyl's signal is much less dependent on temperature, it may serve as a control for nonthermal frequency drifts (11,12). The chemical shift difference between the central resonance frequencies of the water signal and the NAA's methyl signal was calculated using either the peak of the signals in single frames or a least-square fitting on average spectra (four-frames) using a Lorentzian line-shape equation:

$$L(\omega) = (1/T_2^*)/((1/T_2^*)^2 + (\omega - \omega_0)^2) \quad [1]$$

where  $\omega_0$  is the center of resonance. The difference between the center of resonance of the water signal and that of the NAA signal, and the  $T_2^*$  values were calculated only in the spectra in which the fit of both signals to the Lorentzian equation yielded  $R^2 > 0.9$ . Brain temperature in degrees Celsius was calculated according to (11):

$$T = 286.9 - 94.0 \times (\delta_{\text{water}} - \delta_{\text{NAA}}) \quad [2]$$

Where  $\delta_{\text{water}}$  is the center of resonance of the water signal, and  $\delta_{\text{NAA}}$  is the center of resonance of the NAA signal, in ppm. The sensitivity of this MR thermometry method is 0.0106 ppm per  $1^\circ\text{C}$  (11,12). In the current study the digital resolution of the water and NAA signals was 0.61 Hz (after zero-filling), and the central frequency was determined by curve-fitting using at least 30 points per signal. The ability to detect the center of the lines was not limited by digital resolution because the intrinsic width of the signals ( $\sim 8$  Hz) was greater than the digital resolution. Using this approach, with sufficient signal-to-noise ratio (SNR), the center of the lines was found to be much better than a digital resolution by the curve-fitting. The SNR limits of the center frequency measurement appear in the standard deviation (SD), which is part of the statistical analysis.

These spectral analyses were performed in MATLAB (The MathWorks, Inc., Natick, MA, USA).

#### Metabolite and Neurotransmitter Concentration

Analysis of the metabolite and neurotransmitter concentration was performed using LC-Model (Stephen Provencher Inc., Oakville, Ontario, Canada) embedded in SAGE (GE Medical Systems). For each cycle (four dummy scans and 48 MRS frames) the frames were grouped into three block categories according to the stimulation paradigm: rest, stimulation, and post-stimulation. For each subject the spectra of the 10 cycles were combined according to their category, yielding three averaged spectra, each of 160 frames (5.3 min) of rest, stimulation, and post-stimulation. Metabolite-to-creatine (Cr) ratios were determined in these three spectra for each subject. Metabolite

concentrations and SNR were calculated assuming 10 mM Cr, which is an approximate median of the range of previously published values in gray matter (13,14). The use of a short TE combined with a high magnetic field and a small region of interest (ROI, 4  $\text{cm}^3$ ) enabled a more precise determination of glutamate (Glu) and glutamine (Gln) by the LC-model fitting algorithm (15).

In summary, the metabolic study was carried out using the same raw data that were used for the temperature study. However, the data were processed differently in terms of data set formation and spectral analysis. The data set for the metabolic study was comprised of one sample point (one averaged spectrum of 160 frames) per period (stimulation or rest) per subject, as opposed to 40 sampling points (averages of four frames) per period per subject in the temperature study. The metabolic spectral analysis was carried out using LC-Model, which is a multisignal curve-fit procedure, as opposed to the Lorentzian line-fit of individual signals in the temperature analysis.

#### Statistical Analysis

Statistical analysis was performed with StatView (SAS Institute Inc., Cary, NC, USA). Differences among rest, stimulation, and post-stimulation were analyzed by ANOVA ( $\alpha = 5\%$ ). Specific differences between two groups (stimulation – rest and post-stimulation – rest) and 95% confidence intervals (CI) for these differences were determined using paired two-tailed *t*-tests.

## RESULTS

All of the subjects showed a strong fMRI signal enhancement response to the stimulation, which was observed in the striate cortex as well as in the extrastriate cortices. The response was similar prior to and at the end of the study, ruling out acclimation to the stimulus as a result of the consecutive MRS recordings (Fig. 1).

#### Frequency, Temperature, and $T_2^*$ Variations

The frequency variations of the water and the metabolites signals were similar but did not correlate with the stimulation paradigm (Fig. 2). The frequency of the 10th cycle was significantly lower than that of the first cycle for all of the investigated signals ( $P = 0.021, 0.0058, 0.013,$  and  $0.0041$  for water, Cho, Cr, and NAA, respectively; two-tailed paired *t*-test,  $N = 9$  subjects). The average frequency decrease, estimated from the difference of the mean frequency in the 10th and first cycles for each subject, was  $0.11 \pm 0.12, 0.13 \pm 0.11, 0.13 \pm 0.12,$  and  $0.13 \pm 0.10$  Hz/min for the water, Cho, Cr, and NAA signals, respectively.

In contrast to these global frequency shifts, the chemical shift difference between the water signal and the NAA signal was found to be stable throughout the time course of the experiment (Fig. 3). For a more accurate determination of the central frequency of each signal and the difference between them, the lines were fitted to a Lorentzian curve (see Materials and Methods). To achieve a good fit for the NAA signal ( $R^2 > 0.9$ ), fitting was performed on averaged spectra (four frames). Typical water and NAA signals at rest and during stimulation are shown in Fig. 4. The tem-

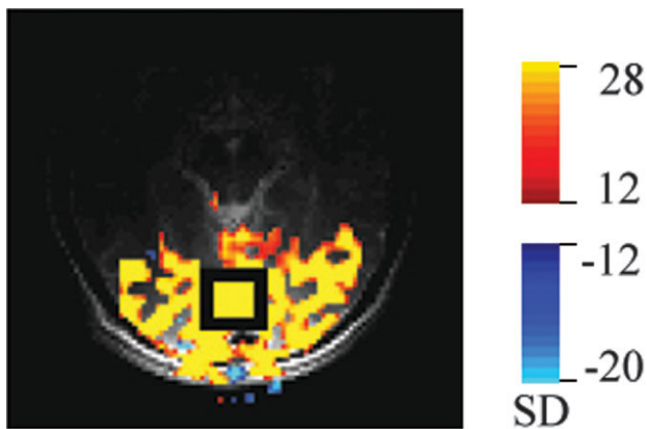


FIG. 1. fMRI of visual cortex stimulation: a typical BOLD response to the visual stimulus in one of the subjects. The statistical map was overlaid on the  $T_2$ -weighted image. The position of the MRS voxel is indicated by a black square. The use of optimized conditions (3T magnet, optimal size surface coil, and positioning of the calcarine sulcus at the middle of the coil), as well as a robust visual stimulation paradigm, enabled the recording of a strong response from the extrastriate cortices in addition to the striate cortex. These conditions were also advantageous for obtaining high-quality spectroscopic data. Note that a large part of the brain is not visible in the anatomic  $T_2$ -weighted image, in agreement with the surface coil's response profile.

perature of the visual cortex at rest (see Materials and Methods) was found to be  $36.6 \pm 0.8^\circ\text{C}$  ( $N = 9$  subjects). The mean difference in temperature during stimulation was  $0.1^\circ\text{C}$  (95% CI =  $0-0.2^\circ\text{C}$ ,  $P = 0.09$ , paired two-tailed  $t$ -test), which suggests that the temperature of the visual cortex did not change significantly during activation. In the period post-stimulation, the temperature remained unchanged (Table 1).

The curve-fit of the NAA signal also provided the  $T_2^*$  value of this signal (see Eq. [1]). At rest the  $T_2^*$  of the NAA signal was  $64 \pm 9$  ms. During stimulation this value did not change significantly within a 95% CI of  $-3\%$  to  $5\%$ .

#### Metabolite and Neurotransmitter Concentration

Figure 5a demonstrates a typical spectrum of one of the subjects showing prominent signals of the metabolites and neurotransmitters of the brain. The total pools of brain metabolites and neurotransmitters were similar during rest, stimulation, and post-stimulation as shown in Fig. 5b. Differences in concentration during stimulation ranged from 0.5% to 3.6% of the rest values for Glu, NAA, choline (Cho), myo-Inositol (ml), and Gln; 7.1% for lactate (Lac); and 46% for Glc (Fig. 5b). However, none of these differences were strongly significant (ANOVA,  $P > 0.7$ ; paired two-tailed  $t$ -test,  $P > 0.1$ ; Table 1). The concentration post-stimulation was not significantly different from either the stimulation or the rest values (ANOVA,  $P > 0.7$ ; paired two-tailed  $t$ -test,  $P > 0.1$ ; Table 1). These results suggest that the concentration of these brain metabolites did not change as a result of activation, within the limits on their determination (Table 1).

#### DISCUSSION

Heat in the brain is produced mostly by oxidative metabolism and is removed chiefly by blood flow (9,16). The

time that characterizes temperature changes in the brain is determined largely by the regional CBF (rCBF) (9). The dynamic bio-heat equation (9,16) describes the rate of temperature change in the brain when the resting state is disturbed by changes in rCBF,  $f$ , incoming blood temperature,  $T_{\text{blood}}$ , or tissue heat generation,  $Q$ :

$$C_{\text{tissue}} dT/dt = Q - \rho_{\text{blood}} C_{\text{blood}} f (T - T_{\text{blood}}) \quad [3]$$

where  $C_{\text{tissue}}$  is the heat capacity of the tissue,  $T$  is the tissue temperature,  $\rho_{\text{blood}}$  is the blood density, and  $C_{\text{blood}}$  is the blood heat capacity. Since  $C_{\text{blood}}$  and  $C_{\text{tissue}}$  are approximately equal and  $\rho_{\text{blood}}$  is approximately 1 g/ml, a change in the flow will cause a change in temperature with a time constant  $1/f$ . For gray matter flow of 80 ml/100 g/min at rest elevated by 50% to 120 ml/100 g/min, the characteristic time constant is 50 s. Thermal conduction would further decrease this time. By 32 s, at least half of the total temperature change is expected to occur. The block design paradigm used here (with 118 s between stimulation periods) was therefore suitable for the repeated monitoring of temperature changes in the cortex.

The shift in the central resonance frequency of the water signal, as determined by MRI or MRS, is the basis for the majority of studies on MR thermometry (that do not use an invasive administration of a contrast agent). It is currently the predominant available noninvasive indicator of temperature in deep-brain regions. However, here the frequency shifts of the water signal were found to be due to a global, nonthermal source, and were uncorrelated to the

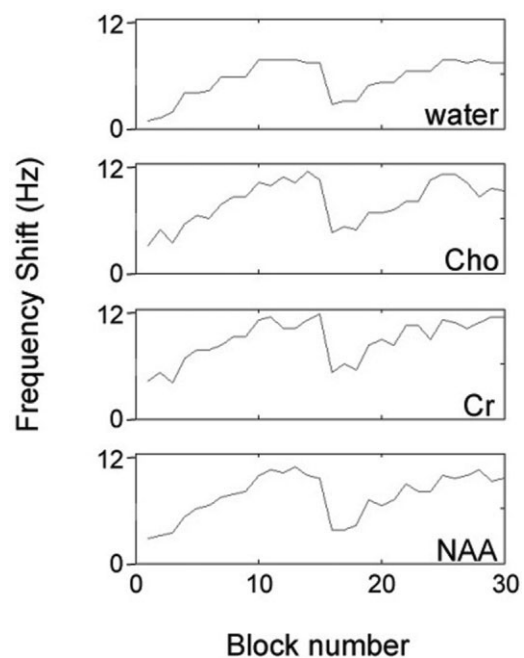
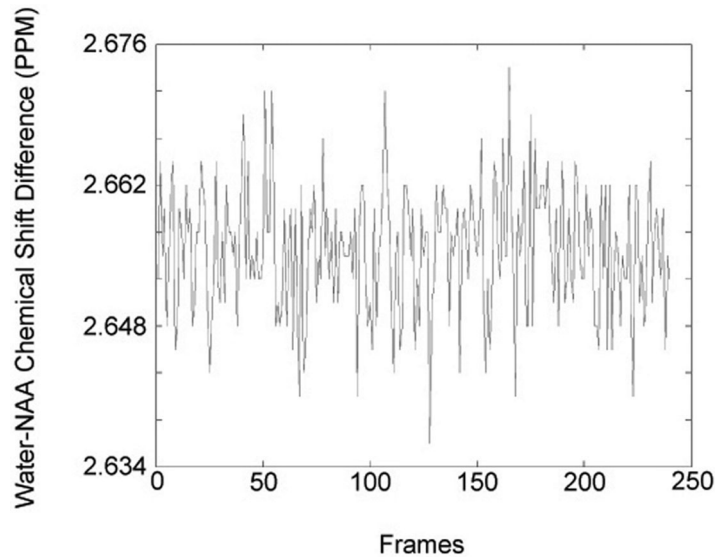


FIG. 2. A typical time course of frequency shifts in one of the subjects. The individual frequency shifts of the water, Cho, Cr, and NAA signals are shown. Block number refers to the average of 16 frames. The data are shown starting with the first rest period (block number 1) and ending with the last post-stimulation period (block number 30). The starting point on the frequency shift scale is arbitrary.

FIG. 3. Time course of the chemical shift difference between the water and the NAA signals in one of the subjects. The results of every second acquisition frame are shown. The first eight frames were acquired during rest, the subsequent eight frames were acquired during stimulation, and the subsequent eight frames were acquired during the post-stimulation period, with this order repeating for 10 cycles. In this analysis the chemical shift difference was evaluated in each single frame using the peaks of the signals as indicators of their central resonance frequencies.



stimulation paradigm. The potential causes for such frequency shifts include magnetic field drifts and susceptibility changes, as well as subject motion. The NAA signal served as a control for the nonthermal changes in fre-

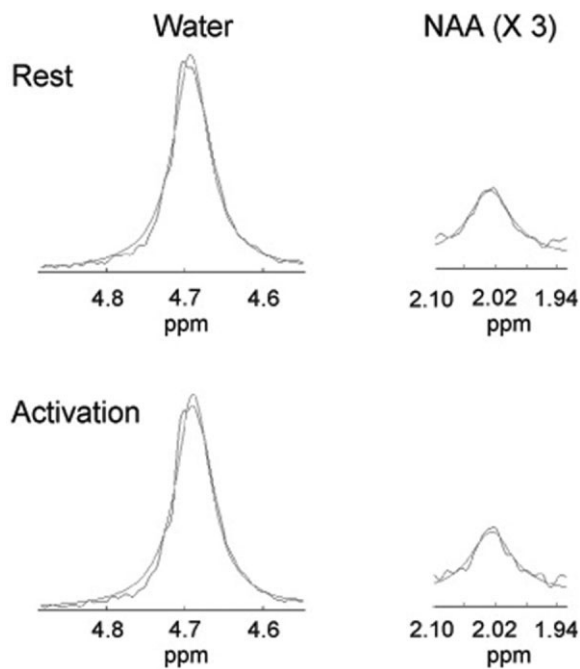


FIG. 4. Typical curve-fitting of the water and the NAA signals in the primary visual cortex of one of the subjects at rest and during stimulation. The curve-fit of these signals enabled robust determination of their central resonance frequency. The chemical shift difference between the central resonance frequencies of these signals was used in the temperature calculation. The curve-fit procedure was applied on averaged spectra of four frames (8 s of acquisition in a 4 cm<sup>3</sup> voxel). The least-square curve-fit was calculated using a Lorentzian line shape (Eq. [1]). The criterion for including the curve-fit results in the statistical analysis of temperature changes was  $R^2 > 0.9$  for both the water and the NAA signals. This procedure was also used to determine the  $T_2^*$  of NAA. The NAA signal was enlarged threefold relative to the water signal.

quency. This approach was developed and validated about 10 years ago (11,12), and has been used since in various applications. Using this approach in combination with the behavioral paradigm, the temperature of the visual cortex was found to be unaffected or slightly increased during stimulation, within a 95% CI of 0–0.2°C. Without the NAA control, our data would have been extremely corrupted by the nonthermal changes in frequency. Our results are in agreement with the results of a model for human brain temperature that includes the effects of metabolism, perfusion, and thermal conduction, and predicted that the maximal change in regional brain temperature would be 0.12°C (16). This result appears to be the most relevant comparison to the current study. A previous noninvasive MR study of human brain temperature reported an average decrease of 0.2°C in the visual cortex (9). However, this decrease was observed only after at least 1 min of stimulation and the study did not use a metabolite control for nonthermal frequency shifts. Other studies in humans used invasive techniques, such as infrared probes directed at the exposed cortical surface (17,18). However, deep-brain regions could not be investigated with this technique. Studies of brain temperature in rodents used various techniques, including direct thermocouple determination of temperature in deep-brain regions (16). However, the differences in brain size and blood flow rate, which lead to differences in thermal conduction and convection, may render a different effect of activation in deep-brain regions of rodents compared to humans.

Our constraints on temperature change during activation suggest that important increases in heat production occur during activation. Except for very near the edge of the brain, temperature control is determined predominantly by local heat production and inflow of blood at an approximately 0.3°C lower temperature than the brain parenchyma (9,16). Visual stimulation induces up to 50% increases in blood flow and Glc utilization across a relatively large volume of the visual cortex (19). A 50% increase in flow should induce a 0.1°C temperature drop in the absence of increased heat production. Our constraints

Table 1  
Limits on Activation-Induced Changes in Temperature and Metabolite Concentrations\*

	At rest	Difference: stimulation-rest		Difference: poststimulation-rest	
		Mean	95% CI and <i>P</i> -value	Mean	95% CI and <i>P</i> -value
Temperature (°C)	36.6 ± 0.8	0.1	0 to 0.2, <i>P</i> = 0.09	-0.1	-0.4 to 0.3, <i>P</i> = 0.7
Glutamate (mM)	14.9 ± 1.5	0.076	-0.50 to 0.66, <i>P</i> = 0.8	0.26	-0.37 to 0.88, <i>P</i> = 0.4
NAA (mM)	15.5 ± 1.0	-0.23	-0.75 to 0.29, <i>P</i> = 0.3	-0.29	-0.66 to 0.09, <i>P</i> = 0.1
Choline (mM)	1.4 ± 0.1	-0.02	-0.08 to 0.03, <i>P</i> = 0.4	-0.03	-0.09 to 0.03, <i>P</i> = 0.2
Myo-Inositol (mM)	5.2 ± 0.7	-0.18	-0.45 to 0.09, <i>P</i> = 0.2	-0.12	-0.36 to 0.12, <i>P</i> = 0.3
Glutamine (mM)	5.6 ± 1.9	-0.20	-1.22 to 0.82, <i>P</i> = 0.7	0.23	-1.3 to 1.8, <i>P</i> = 0.8
Lactate (mM)	1.1 ± 0.5	-0.08	-0.65 to 0.49, <i>P</i> = 0.8	-0.11	-1.1 to 0.83, <i>P</i> = 0.8
Glucose (mM)	0.5 ± 0.9	-0.23	-0.54 to 0.08, <i>P</i> = 0.1	-0.22	-0.62 to 0.18, <i>P</i> = 0.2

\*ANOVA analysis of both the temperature and the metabolic data did not yield any significant differences, with all *P* values greater than 0.7. Paired two-tailed *t*-tests were carried out to determine the 95% confidence intervals (CI) of the specific differences. Values at rest are given as mean ± SD, *N* = 9 subjects.

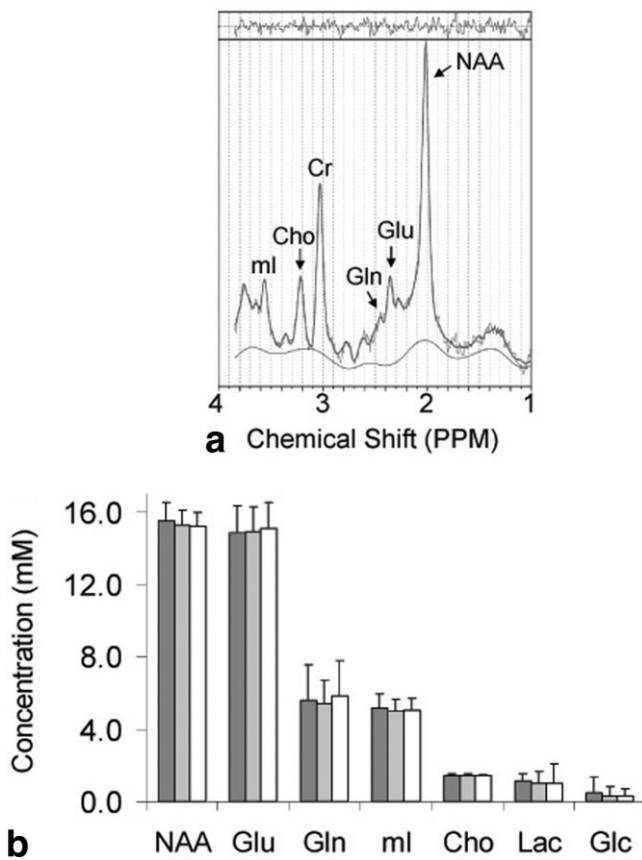


FIG. 5. Typical MRS spectrum of the visual cortex and summary of metabolite and neurotransmitter concentrations during rest, stimulation, and post-stimulation. **a**: A typical MRS spectrum of the visual cortex acquired during 10 stimulation periods (5.3 min) in one of the subjects. The standard output of the LC-Model spectra analysis software is shown. In the lower part of the panel, the thin line shows the raw spectrum without postprocessing, the thick line shows the result of the fit, and the smoother thin line shows the baseline calculated by the fitting algorithm. The residual of the fit is shown in the upper part of the panel. **b**: Concentration of metabolites and neurotransmitters in the primary visual cortex. The means of the results from nine subjects during rest (dark gray), stimulation (light gray), and post-stimulation (white) are shown. The error bars represent 1 SD.

on temperature change, however, suggest an increase in heat production that is proportional to or even greater than the increase in flow. Were this increase to result from metabolic consumption of the increased Glc utilized, almost completely aerobic metabolism of this Glc would be required because of the limited heat produced by glycolysis. This conclusion is in agreement with a study that employed carbon-13 MRS monitoring of the regional tricarboxylic acid cycle flux in humans, which showed that cerebral Glc is metabolized oxidatively even during intense visual stimulation (20). The elevated oxygen consumption required, however, would be in disagreement with almost all studies of oxygen utilization changes accompanying activation. Alternatively, neural activity itself may be exothermic (21). While any heat produced during activity must eventually be replaced by Glc metabolism, the time scale for full replenishment of cellular ion concentrations could be many hours. The approximately proportionate increases in heat production and flow indicated by our results suggest that flow elevation during activation may serve primarily to remove increased heat and regulate temperature during activation.

A methodological note regarding water suppression deserves attention with respect to brain activation. We applied water suppression to reduce the water signal to a level comparable to that of the metabolite signals in order to determine the central resonance frequencies of both the water and the NAA signals at the same level of precision. However, the line shape of the resulting residual water signal may have been altered by the water suppression. Therefore, the line width of this signal or the calculated  $T_2^*$  of this signal could not serve as a reliable measure of the water oxygenation level during activation. Nevertheless, the central resonance frequency of a signal is not dependent on the line shape or the line width of a signal. Therefore, the temperature determination, which relied on determination of the center of the water signal, was not dependent on the water suppression. The determination of the NAA  $T_2^*$  relaxation time did not depend on the water suppression either, because the water-suppression scheme used chemical shift-selective (CHESS) pulses that did not affect the metabolite region of the spectrum.

The  $T_2^*$  of NAA relates to the extravascular effects of blood oxygenation. Since NAA is not present in high concentrations in the blood, a change in the  $T_2^*$  of NAA could

serve as an indicator of  $T_2^*$  changes within the brain tissue, predominantly within neurons. A number of theoretical and experimental investigations (22–25) have predicted that the extravascular effects of blood oxygenation are weaker than the intravascular effects at lower field strength, but become increasingly predominant at higher field strengths. In a previous study a decrease of 1.7% in the line width of the NAA signal during stimulation was reported at 4 T (26). Although our results did not show a significant change in the NAA  $T_2^*$ , the limit of change was well within the range of this previous experimental result and the theoretical calculations. In addition, it should be noted that in Ref. 26 these changes were determined using the width at half height, as opposed to our study, which utilized a curve-fit procedure. These different analysis methods could also lead to the difference in the results.

Although the activation-induced increase in Glc consumption is well established, the metabolic routing of Glc in the activated intact human brain is not fully characterized. Carbon-13 MRS studies have used the fractional change in the turnover rate of C4 carbon of glutamate during visual stimulation as an index of alterations in the neuronal TCA cycle turnover during increased neuronal activity (27). The results of Ref. 27 suggested that the fractional changes in  $\text{CMR}_{\text{O}_2}$  induced by activation were no higher than 30%. In rat brain slices the astrocytic anaerobic glycolysis was found to start after 8 s of stimulation (10). However, it should be noted that both oxidative and anaerobic glycolysis have been found to be enhanced in brain-slice preparations compared to intact brain (28). Monitoring of Lac production by MRS has been suggested as a way to directly monitor nonoxidative Glc consumption in the activated human brain (4–6). Our results underscore the challenges of accurately characterizing Lac accumulation during activation. The maximum Lac production rate, optimum sampling time, and sensitivity of MRS for Lac are discussed below.

In this study no increase in Lac concentration was observed during stimulation. However, this result may have been related to the use of the block design paradigm (32-s stimulation duration). Because the samples (frames) from zero through 32 s of stimulation were combined to increase the SNR, the effective stimulation time that was sampled in one stimulation period was 16 s. We examine the potential Lac increase in 16 s in the following sections.

Reported values of the resting-state cerebral metabolic rate (CMR) of Glc ( $\text{CMR}_{\text{glc}}$ ) in anesthetized and awake rats range from 0.17 to 0.8  $\mu\text{mol/g/min}$  for the combined oxidative and nonoxidative routes (29–34), and a rate of 0.37  $\mu\text{mol/g/min}$  has been reported in humans (19). Oxidative  $\text{CMR}_{\text{glc}}$  can also be estimated from values of the regional CMR of oxygen ( $\text{rCMRO}_2$ ). The average  $\text{rCMRO}_2$  in the human brain is 1.5  $\mu\text{mol/g/min}$  (9), corresponding to an oxidative  $\text{CMR}_{\text{glc}}$  of 0.25  $\mu\text{mol/g/min}$ . The reported increase in  $\text{CMR}_{\text{glc(oxidative or total)}}$  ( $\Delta\text{CMR}_{\text{glc}}$ ) in the human primary visual cortex during activation ranges from 23% to 51% (1). Considering the resting-state  $\text{CMR}_{\text{glc}}$  of 0.25  $\mu\text{mol/g/min}$  and a maximal  $\Delta\text{CMR}_{\text{glc}}$  in the human brain of 51%, and assuming that all of the increase in consumed Glc has been routed to Lac production without clearance, the upper limit for the rate of Lac accumulation during activation is 0.255  $\mu\text{mol/g/min}$ . Therefore, a maximum

of 0.068 mM of Lac would be expected to accumulate in 16 s (assuming a volume of 1 ml for 1 g of brain tissue). According to our results, a change of this magnitude could not have been significantly determined (Table 1). Hence, the limits on Lac concentration changes were too weak to constrain theories of elevated anaerobic Glc utilization during stimulation. Increased astrocytic anaerobic glycolysis has been shown to start after 8 s of stimulation and last for more than 2 min after the stimulation (10). Therefore, in the absence of efflux, Lac accumulation should occur in the 32-s period post-stimulation. The effective time for Lac accumulation in the post-stimulation spectra is 40 s ( $32 - 8 + 32/2$ ). According to the above calculation, the amount of Lac that is expected to accumulate during this time is 0.170 mM. The limits on Lac concentration changes during the post-stimulation period were also too weak to significantly determine a change of this order of magnitude (Table 1).

Previous MRS studies of human visual stimulation disagree on the changes in Lac that occur during activation. Increases of 0.3–0.9 mM in 6 min (4), 0.26 mM in 2.5 min (6), and 250% at 6.4 min (5) have been reported. However, in another study the pattern of the Lac accumulation was not reproducible, and some subjects showed no increase or a decrease in Lac levels (35). In a more recent study that used  $^1\text{H}$  chemical shift imaging, signals at 1.33 ppm were concluded to be artifactual, originating from lipid signals from outside the volume of interest, and did not change upon visual stimulation (36). Large and transitory decreases in the Lac level at 5 s from visual stimulation onset have been reported (37), but such rapid changes would require a different mechanism. In anesthetized cats, no Lac peak was observed in the visual cortex during 70 s of visual activation (38). In summary, our results, combined with these previous reports, indicate that Lac changes are challenging to detect even with long stimulation.

An increase of up to 30% in the Glu labeling rate was previously found during stimulation in the awake resting human brain (27). This change in the rate of neurotransmitter cycling during activation could potentially affect the total pool concentration of Glu. For this reason we tested the difference in Glu concentration during stimulation and post-stimulation (Table 1). We used the same calculation as above to predict the expected change in Glu concentration as a result of activation, ignoring clearance and further metabolism. For a maximal  $\Delta\text{CMR}_{\text{glc}}$ , an increase of 0.068 mM Glu is expected in 16 s. Indeed, we found an increase of 0.076 mM in Glu concentration (Table 1), but the limits on Glu concentration changes were too weak to determine this change significantly.

A 40% decrease in the Glc level during activation was previously reported (6,35). The current results suggest a similar decrease of 46%, but since the Glc signals were mostly below the detection level, this decrease was not significant and relies on the results of a small number of subjects. It should be noted that for multiplet signals of low quantity that overlap with other signals, such as Lac and Glc, the error in concentration determination was large (Fig. 5, Table 1). The SNR of the Cr signal was 4.0 per mM per min acquisition per 4  $\text{cm}^3$  voxel. Because the Lac signal is a doublet, its corresponding SNR would be 2.0. Literature values for resting-state Lac range from 0.5 to

1 mM (4,39,40). Accurate determination of 1 mM Lac (SNR of least 10) would require an acquisition time of 25 min, which is impractical for activation studies. Since the signals of Glc are more complex multiplets, an even longer time would be required for an accurate determination of the Glc content. Thus, the concentrations of Lac and Glc are given here as upper limits and not as measured concentrations.

One potential way to increase the SNR for a given stimulation duration would be to increase the spectroscopic voxel size. In this study, however, the spectroscopic data were acquired from a small single voxel (4 cm<sup>3</sup>) localized in the center of the activated region. This strategy, as opposed to the use of a larger single voxel or a small voxel in a CSI map, was chosen in order to limit the influence of nonactivated regions on the results. Ideally, the SNR of the MRS signals is linearly dependent on voxel volume; however, in clinical investigations at high field, the reduction in SNR due to smaller voxel volume is less pronounced because of the greater inhomogeneity in larger voxels. Larger voxels centered at the calcarine fissure may also include blood vessels, which were avoided here.

In summary, limits on changes in temperature,  $T_2^*$  relaxation time, and metabolite and neurotransmitter concentrations were all determined simultaneously by partially water-suppressed MRS at high field using a stimulation paradigm similar to that of a typical block-design fMRI study. These physiologic and metabolic properties appear to be unaffected by brain activation. Constraints on the temperature change, however, suggest a large increase in metabolic heat production accompanying activation.

## REFERENCES

- Buxton RB. An introduction to functional magnetic resonance imaging: principles and techniques. Cambridge: Cambridge University Press; 2002. p 3–41.
- Erickson KM, Lanier WL. Anesthetic technique influences brain temperature, independently of core temperature, during craniotomy in cats. *Anesth Analg* 2003;96:1460–1466.
- Logothetis NK, Pauls J, Augath M, Trinath T, Oeltermann A. Neurophysiological investigation of the basis of the fMRI signal. *Nature* 2001;412:150–157.
- Prichard J, Rothman D, Novotny E, Petroff O, Kuwabara T, Avison M, Howseman A, Hanstock C, Shulman R. Lactate rise detected by H-1-NMR in human visual-cortex during physiological stimulation. *Proc Natl Acad Sci USA* 1991;88:5829–5831.
- Sappey-Marinié D, Calabrese G, Fein G, Hugg JW, Biggins C, Weiner MW. Effect of photic-stimulation on human visual-cortex lactate and phosphates using H-1 and P-31 magnetic-resonance spectroscopy. *J Cereb Blood Flow Metab* 1992;12:584–592.
- Frahm J, Kruger G, Merboldt KD, Kleinschmidt A. Dynamic uncoupling and recoupling of perfusion and oxidative metabolism during focal brain activation in man. *Magn Reson Med* 1996;35:143–148.
- Urrilla AS, Hakkarainen T, Heikkinen T, Vuori T, Stenberg D, Hakkinen AM, Lundbom T, Porkka-Heiskanen T. Metabolic imaging of human cognition: an fMRI/H-1-MRS study of brain lactate response to silent word generation. *J Cereb Blood Flow Metab* 2003;23:942–948.
- Richards TL, Dager SR, Corina D, Serafini S, Heide AC, Steury K, Strauss W, Hayes CE, Abbott RD, Craft S, Shaw D, Posse S, Berninger VW. Dyslexic children have abnormal brain lactate response to reading-related language tasks. *AJNR Am J Neuroradiol* 1999;20:1393–1398.
- Yablonskiy DA, Ackerman JH, Raichle ME. Coupling between changes in human brain temperature and oxidative metabolism during prolonged visual stimulation. *Proc Natl Acad Sci USA* 2000;97:7603–7608.
- Kasischke KA, Vishwasrao HD, Fisher PJ, Zipfel WR, Webb WW. Neuronal activity triggers neuronal oxidative metabolism followed by astrocytic glycolysis. *Science* 2004;305:99–103.
- Cady EB, Dsouza PC, Penrice J, Lorek A. The estimation of local brain temperature by in-vivo H-1 magnetic-resonance spectroscopy. *Magn Reson Med* 1995;33:862–867.
- Corbett RJ, Laptook AR, Tollefsbol G, Kim B. Validation of a noninvasive method to measure brain temperature in vivo using 1H NMR spectroscopy. *J Neurochem* 1995;64:1224–1230.
- Knight-Scott J, Haley AP, Rossmiller SR, Farace E, Mai VM, Christopher JM, Manning CA, Simnad VI, Siragy HM. Molality as a unit of measure for expressing 1H MRS brain metabolite concentrations in vivo. *Magn Reson Imaging* 2003;21:787–797.
- Pouwels PJ, Brockmann K, Kruse B, Wilken B, Wick M, Hanefeld F, Frahm J. Regional age dependence of human brain metabolites from infancy to adulthood as detected by quantitative localized proton MRS. *Pediatr Res* 1999;46:474–485.
- Kanowski M, Kaufmann J, Braun J, Bernarding J, Tempelmann C. Quantitation of simulated short echo time 1H human brain spectra by LCModel and AMARES. *Magn Reson Med* 2004;51:904–912.
- Collins CM, Smith MB, Turner R. Model of local temperature changes in brain upon functional activation. *J Appl Physiol* 2004;97:2051–2055.
- Ecker RD, Goerss SJ, Meyer FB, Cohen-Gadol AA, Britton JW, Levine JA. Vision of the future: initial experience with intraoperative real-time high-resolution dynamic infrared imaging. *J Neurosurg* 2002;97:1460–1471.
- Gorbach AM, Heiss J, Kuffa C, Sato S, Fedio P, Kammerer WA, Solomon J, Oldfield EH. Intraoperative infrared functional imaging of human brain. *Ann Neurol* 2003;54:297–309.
- Fox PT, Raichle ME, Mintun MA, Dence C. Nonoxidative glucose consumption during focal physiologic neural activity. *Science* 1988;241:462–464.
- Chhina N, Kuestermann E, Halliday J, Simpson LJ, Macdonald IA, Bachelard HS, Morris PG. Measurement of human tricarboxylic acid cycle rates during visual activation by (13)C magnetic resonance spectroscopy. *J Neurosci Res* 2001;66:737–746.
- Ritchie JM, Keynes RD. The production and absorption of heat associated with electrical activity in nerve and electric organ. *Q Rev Biophys* 1985;18:451–476.
- Duong TQ, Yacoub E, Adriany G, Hu X, Ugurbil K, Kim SG. Microvascular BOLD contribution at 4 and 7 T in the human brain: gradient-echo and spin-echo fMRI with suppression of blood effects. *Magn Reson Med* 2003;49:1019–1027.
- Boxerman JL, Hamberg LM, Rosen BR, Weisskoff RM. MR contrast due to intravascular magnetic susceptibility perturbations. *Magn Reson Med* 1995;34:555–566.
- Silvennoinen MJ, Clingman CS, Golay X, Kauppinen RA, van Zijl PC. Comparison of the dependence of blood R2 and R2\* on oxygen saturation at 1.5 and 4.7 Tesla. *Magn Reson Med* 2003;49:47–60.
- Yablonskiy DA, Haacke EM. Theory of NMR signal behavior in magnetically inhomogeneous tissues: the static dephasing regime. *Magn Reson Med* 1994;32:749–763.
- Zhu XH, Chen W. Observed BOLD effects on cerebral metabolite resonances in human visual cortex during visual stimulation: a functional H-1 MRS study at 4 T. *Magn Reson Med* 2001;46:841–847.
- Chen W, Zhu XH, Gruetter R, Seaquist ER, Adriany G, Ugurbil K. Study of tricarboxylic acid cycle flux changes in human visual cortex during hemifield visual stimulation using H-1-(C-13) MRS and fMRI. *Magn Reson Med* 2001;45:349–355.
- Ting YL, Degani H. Energetics and glucose metabolism in hippocampal slices during depolarization: <sup>31</sup>P and <sup>13</sup>C NMR studies. *Brain Res* 1993;610:16–23.
- Dudley RE, Nelson SR, Samson F. Influence of chloralose on brain regional glucose utilization. *Brain Res* 1982;233:173–180.
- Hyder F, Chase JR, Behar KL, Mason GF, Siddeek M, Rothman DL, Shulman RG. Increased tricarboxylic acid cycle flux in rat brain during forepaw stimulation detected with 1H [13C] NMR. *Proc Natl Acad Sci USA* 1996;93:7612–7617.
- Sokoloff L. Relationships among local functional activity, energy metabolism, and blood flow in the central nervous system. *Fed Proc* 1981;40:2311–2316.
- Ueki M, Linn F, Hossmann KA. Functional activation of cerebral blood-flow and metabolism before and after global-ischemia of rat-brain. *J Cereb Blood Flow Metab* 1988;8:486–494.
- Cohen DM, Wei JN, Smith EO, Gao XL, Quast MJ, Sokoloff L. A method for measuring cerebral glucose metabolism in vivo by C-13-NMR spectroscopy. *Magn Reson Med* 2002;48:1063–1067.

34. Sibson NR, Dhankhar A, Mason GF, Rothman DL, Behar KL, Shulman RG. Stoichiometric coupling of brain glucose metabolism and glutamatergic neuronal activity. *Proc Natl Acad Sci USA* 1998;95:316–321.
35. Merboldt KD, Bruhn H, Hancicke W, Michaelis T, Frahm J. Decrease of glucose in the human visual-cortex during photic-stimulation. *Magn Reson Med* 1992;25:187–194.
36. Boucard CC, Mostert JP, Cornelissen FW, De Keyser J, Oudkerk M, Sijens PE. Visual stimulation, 1H MR spectroscopy and fMRI of the human visual pathways. *Eur Radiol* 2005;15:47–52.
37. Mangia S, Garreffa G, Bianciardi M, Giove F, Di Salle F, Maraviglia B. The aerobic brain: lactate decrease at the onset of neural activity. *Neuroscience* 2003;118:7–10.
38. Kauppinen RA, Eleff SM, Ulatowski JA, Kraut M, Soher B, van Zijl PC. Visual activation in alpha-chloralose-anaesthetized cats does not cause lactate accumulation in the visual cortex as detected by [1H]NMR difference spectroscopy. *Eur J Neurosci* 1997;9:654–661.
39. Gruetter R, Seaquist ER, Kim S, Ugurbil K. Localized in vivo C-13-NMR of glutamate metabolism in the human brain: initial results at 4 Tesla. *Dev Neurosci* 1998;20:380–388.
40. Pfeuffer J, Tkac I, Choi IY, Merkle H, Ugurbil K, Garwood M, Gruetter R. Localized in vivo H-1 NMR detection of neurotransmitter labeling in rat brain during infusion of 1-C-13 D-glucose. *Magn Reson Med* 1999;41:1077–1083.